Mechanical Design of a Feline Robot for Dynamic Scaling Testing

Amy Budzichowski[1], Shane Riddle[1], Rucha Batchu[1], Tina Chen[1], Clayton B. Jackson[1], William R. P. Nourse[2(✉)], and Roger D. Quinn[1]

[1] Department of Mechanical and Aerospace Engineering, Case Western Reserve University, Cleveland, OH 44106-7222, USA
[2] Department of Electrical, Computer, and Systems Engineering, Case Western Reserve University, Cleveland, OH 44106-7222, USA
wnourse05@gmail.com

Abstract. Animal size impacts locomotion, due to its effect on the influence of gravity, inertia, and an animal's internal elasticity and damping. We are developing a cat robot to further explore the impact of these four characteristics on animal locomotion. This paper details the mechanical design of this cat robot's rear limbs, as well as the simulated validation of this design. In future work, we plan to design forelimbs with a floating scapula and test the robot in split-belt treadmill experiments similar to those done in mammalian experiments as we develop its synthetic nervous system controller.

Keywords: Legged robot · Dynamic scaling · Feline

1 Introduction and Background

Animals of different sizes move differently. This is because different forces dominate a creature's movement depending on how large it is. There are four primary forces which affect locomotor strategy: gravitational, inertial, viscous, and elastic forces. Often, two or three forces will dominate an animal's motion, and the others will be negligible [1,16,19,23,33]. Elastic and viscous forces dominate the locomotion of smaller creatures such as insects, while larger animals such as dogs, humans, and horses experience more prominent gravitational and inertial effects. This is due to both their size and the construction of the animals' anatomy. Insects are small enough that gravitational and inertial effects are negligible, and their anatomy contains significant built-in elasticity and damping [22]. Conversely, larger animals' size means that gravitational and inertial effects dominate their locomotion, and any elastic or damping effects from their anatomy are negligible in comparison [18]. We are building a cat robot in order

This work was funded by National Science Foundation (NSF) DBI 2015317 as part of the NSF/CIHR/DFG/FRQ/UKRI-MRC Next Generation Networks for Neuroscience Program.

© The Author(s), under exclusive license to Springer Nature Switzerland AG 2025
N. S. Szczecinski et al. (Eds.): Living Machines 2024, LNAI 14930, pp. 284–298, 2025.
https://doi.org/10.1007/978-3-031-72597-5_20

to augment prior research on the effect of scale in animals of intermediate size. In modeling the fundamental biomechanics of a cat, we can use this cat robot to further explore feline locomotion.

Given that animal locomotion depends on size, and an animal's nervous system controls its motion, it follows that an animal's size affects the structure and function of its nervous system [33]. Our work seeks to explore this interplay between animal size and nervous system structure. Biomimetic robots are uniquely positioned to explore this interaction, as they allow us to validate scientific hypotheses surrounding animal locomotion [26]. By building robots based on leading theories of biomechanics and neural control, we can reverse-engineer animal locomotion, and emulate live animal experiments with robots which operate on similar principles. Because robots do not get tired or have animal experimental use considerations, experiments involving robotic animals can be carried out at far greater scale than those involving live animals. While this does not aim to replace animal testing entirely, the experiments on robots can be used to test theories and design future experiments on the animals. This allows preliminary research into animal locomotion to be carried out at greater scale for comparatively less cost, allowing live animal trials to be used more economically.

Prior work within our lab has explored the biomechanics and neural control of animals at several different scales: Drosophibot [13], MantisBot [34], Puppy [21], and most recently the rat robot [2]. The creation of this cat robot aims to augment the prior scaling work done within the lab by providing a biomimetic robot at a scale in between rat and dog. Additionally, cats are one of the smaller animals to walk upright [7] rather than in a crouched posture, like rats [15], which makes them an interesting animal for scaling studies. This paper explores the mechanical design of the rear limbs of our cat robot, as well as some preliminary testing and validation of the design and motor control algorithm.

2 Methods and Materials

2.1 Motor Selection and Torque Requirements

The motors selected for this robot are the Westwood Robotics Koala BEAR (Westwood Robotics LLC, Westwood, MA) model. These were chosen for their low gear ratio, back-drivability, and torque feedback capabilities, as well as their relatively small form factor ($6.4 \times 6.2 \times 3.7$ cm) and high torque output (3.5 Nm static, 10.5 Nm dynamic). Additionally, the motors have a speed constant of 27.3 RPM/V. With our 24 V power supply, the maximum velocity of the motors is well above the maximum cat joint velocity of 149 RPM [29]. These motors are quasi-direct drive, which allows for relatively straightforward torque control [30]. Thus, the motors are capable of emulating variable stiffness and damping within the motor control code, something that normally requires physical springs and dampers to be added in series with other motors. Other works which have used these motors have reported sufficient control frequencies [24], however it should be noted that the motors are still limited and cannot emulate infinite stiffness or damping properties. Further testing is needed to characterize the valid regions

of stiffness and damping for these motors, as simulated tests show that too large damping commands require motor torques beyond the maximum dynamic torque of the motors. An alternative is to implement discrete passive springs and dampers at the joints. The ability to dynamically change these properties greatly reduces the robot's design complexity and allows these parameters to be changed dynamically instead of requiring physical replacement of components. Thus, these motors allow us to perform studies on the dynamic scale of the robot without changing the hardware. It is important to note that the dynamic scale of the robot refers to the relationship between inertia, stiffness, damping, and temporal properties, along with the kinematic configuration and scale [33]. Changing any one of these properties impacts the dynamic scale of the robot.

A joint torque analysis was performed to determine the expected loads each joint of the robot would experience during a cat-like walking gait, and whether the Koala motor specifications would be sufficient. We used dynamic motion tracking data of a cat walking on a treadmill from Prilutsky et al. [29]. This data consisted of the limb joint angles and the dynamic force experienced at each joint over time. It also included the mass, length, and center of mass of each part of the limb (digits, tarsal, tibia/fibula, and femur). The vertical force experienced at the metatarsophalangeal (MTP) joint was used to approximate the ground reaction force (GRF), as this element is in contact with the ground during the entirety of stance phase, excluding toe-off.

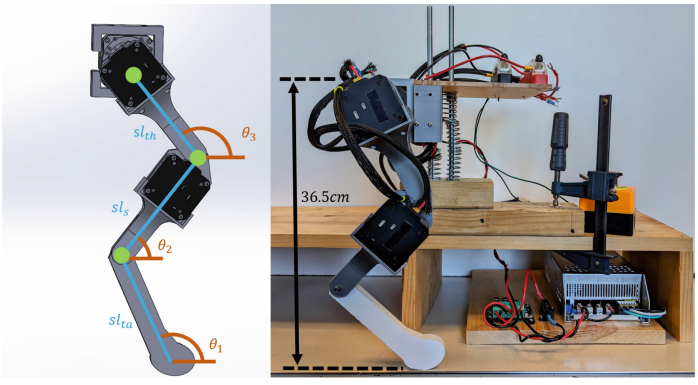

Fig. 1. On the left is a CAD model of the robotic leg. On the right is the physical robotic leg. Green dots represent pivot points, Blue lines represent the limb length. (Color figure online)

The joint torque analysis was performed using forward kinematic, static torque calculations on the model shown in Fig. 1 for each timestep of the collected data tracking the MTP joint angle, the ankle angle, and the knee angle. The static torque calculations used for the initial design phase incorporate the dynamic forces recorded in the motion tracking data giving us the instantaneous torque at each timestep. We recognize that while this provides an estimate for

preliminary design work a true dynamic analysis will need to be performed prior to finalizing the design. To accommodate the use of absolute coordinates in the models, the joint angle data was converted from its initial relative coordinates to absolute coordinates $(\theta_1, \theta_2, \theta_3)$. The robot shown in Fig. 1 has its mass concentrated at the motors, which are located near the joints. This is a reasonable approximation for the purposes of this analysis as the robot limbs are composed of 3D printed carbon fiber and are thus negligibly light compared to the motor mass (250 g).

$$\tau_{\mathrm{ank,c}} = -F_{\mathrm{c}} l_{\mathrm{ta}} \cos(\theta_1) + g\Big[m_{\mathrm{ta}} l_{\mathrm{com,ta}} \cos(\theta_1) + m_{\mathrm{s}}(l_{\mathrm{s}} - l_{\mathrm{com,s}}) \cos(\theta_2) + m_{\mathrm{th}}\Big(l_{\mathrm{s}} \cos(\theta_2) + (l_{\mathrm{th}} - l_{\mathrm{com,th}}) \cos(\theta_3)\Big)\Big] \tag{1}$$

$$\tau_{\mathrm{knee,c}} = -F_{\mathrm{c}}\big[l_{\mathrm{ta}} cos(\theta_1) + l_{\mathrm{s}} cos(\theta_2)\big] + g\Big[m_{\mathrm{ta}}\Big(l_{\mathrm{com,ta}} cos(\theta_1) + l_{\mathrm{s}} cos(\theta_2)\Big) + m_{\mathrm{s}} l_{\mathrm{com,s}} cos(\theta_2) + m_{\mathrm{th}}\Big(l_{\mathrm{th}} - l_{\mathrm{com,th}}\Big) cos(\theta_3)\Big] \tag{2}$$

$$\begin{aligned}\tau_{\mathrm{hip,c}} \; &= -F_{\mathrm{c}}\Big[l_{\mathrm{ta}} cos(\theta_1) + l_{\mathrm{s}} cos(\theta_2) + l_{\mathrm{th}} cos(\theta_3)\Big] \\ &\quad + g\Big[m_{\mathrm{ta}}\Big(l_{\mathrm{com,ta}} cos(\theta_1) + l_{\mathrm{s}} cos(\theta_2) + l_{\mathrm{th}} cos(\theta_3)\Big) \\ &\quad + m_{\mathrm{s}}\Big(l_{\mathrm{com,s}} cos(\theta_2) + l_{\mathrm{th}} cos(\theta_3)\Big) + m_{\mathrm{th}} l_{\mathrm{com,th}} cos(\theta_3)\Big]\end{aligned} \tag{3}$$

Equations 1–3 describe the torque about each joint of the biological cat which inspired our robot, while Eqs. 5–7 describe the torque about each joint of the modeled cat robot. Descriptions and values for each parameter used in these equations can be found in Table 1.

$$F_{\mathrm{r}} = F_{\mathrm{c}} \frac{m_{\mathrm{robot}}}{m_{\mathrm{cat}}} \tag{4}$$

$$\tau_{\mathrm{ank,r}} = s\Big[-F_{\mathrm{r}} l_{\mathrm{ta}} cos(\theta_1) + mgl_{\mathrm{s}} cos(\theta_2)\Big] \tag{5}$$

$$\tau_{\mathrm{knee,r}} = s\Big[-F_{\mathrm{r}}\Big(l_{\mathrm{ta}} cos(\theta_1) + l_{\mathrm{s}} cos(\theta_2)\Big) + mgl_{\mathrm{s}} cos(\theta_2)\Big] \tag{6}$$

$$\tau_{\mathrm{hip,r}} = s\Big[-F_{\mathrm{r}}\Big(l_{\mathrm{ta}} cos(\theta_1) + l_{\mathrm{s}} cos(\theta_2) + l_{\mathrm{th}} cos(\theta_3)\Big) + mg\Big(l_{\mathrm{s}} cos(\theta_2) + 2l_{\mathrm{th}} cos(\theta_3)\Big)\Big] \tag{7}$$

To account for the difference in lengths between the robot and the animal, a scaling factor, s, was incorporated into Eqs. 5–7. To adjust the ground reaction forces (GRFs), the contact forces measured in testing [29], F_c, were scaled by the

ratio of the mass of the robot to the mass of the cat. While compact, the motors were still too large to fit on a frame the size of a typical cat so a length increase was necessary. The length scaling factor allowed us to analyze the increased joint torques the system would experience at larger scales and determine a size that accommodated ease of manufacturing without exceeding the motor torque limits all while trying to keep the scale as close to 1 as possible. The motor masses were placed at the distal end of the femur and tibia of the model for this analysis.

Table 1. The parameters and variables used in the joint torque equations. Variables without listed values are time dependent.

Param.	Description	Value	Param.	Description	Value
θ_1	MTP Joint Angle	–	l_{ta}	Tarsal Length	6.15 cm
θ_2	Ankle Angle	–	l_{s}	Shank Length	9.5 cm
θ_3	Knee Angle	–	l_{th}	Thigh Length	9.4 cm
m_{ta}	Tarsal Mass	19.1 g	$l_{\mathrm{com,ta}}$	Tarsal COM	2.99 cm
m_{s}	Shank Mass	56.1 g	$l_{\mathrm{com,s}}$	Shank COM	4.02 cm
m_{th}	Thigh Mass	142 g	$l_{\mathrm{com,th}}$	Thigh COM	4.16 cm
m_{robot}	Robot Mass	10 kg	τ_{c}	Cat Joint Torque	–
m_{cat}	Cat Mass	3.02 kg	τ_{r}	Robot Joint Torque	–
F_{c}	Contact Force	–	s	Length Scaling Factor	1.75

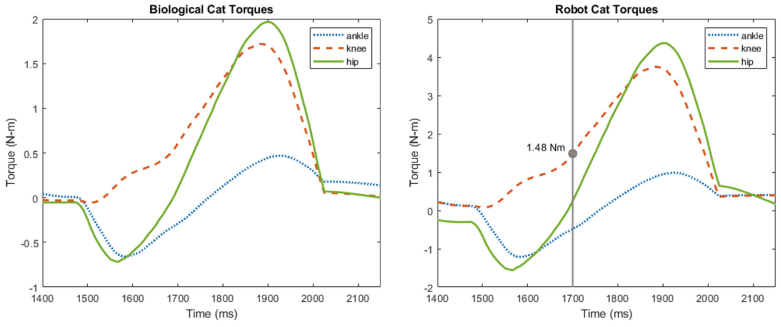

Fig. 2. Hip, knee, and ankle torques through a single stance phase for a cat hind leg and robotic cat leg analogue. The gray line indicates the timestep we considered to be standing position and the maximum torque at that time. The torque profiles are similar in shape but differ in magnitude.

The joint torques over the course of a single stance phase are shown in Fig. 2 for the animal and robot models, respectively. The length scale for the robot model used was 1.75 and the mass of the robot was set to its expected total of 10 kg. Preliminary testing and prototyping revealed that a scale factor of roughly 1.75 was the minimum length increase needed to fit our motors on the robot

without requiring us to manufacture custom drive components, such as the belts and pulleys. To check that this scale produced joint torques within the motor limits we identified a timestep in the stance data where the joint angles correlated to those of a typical standing position (t = 1700 ms). The maximum joint torque calculated at this standing position was 1.48 Nm, well below the motor's static loading limit of 3.5 Nm. Furthermore, the maximum torque experienced over the entirety of stance was under 4.5 Nm, which is well below the motor's dynamic loading limit of 10.5 Nm. With both conditions satisfied, a length scale of 1.75 was chosen for the design of the cat robot. Assuming the motors are placed at the ankle and knee of the robot, this provides enough space to fit them without overloading the motors beyond their torque specification. While the scaling factor would ideally be closer to 1, increasing the amount of space for the motors, without exceeding their torque capabilities, was crucial for manufacturability. An increase in size still allows for the robot to be dynamically similar to the cat because the stiffness and damping in the motors can be increased relative to the inertia of the leg according to scaling laws. Additionally, the robot at a 1.75 scale is still within the size range of domestic felines, falling around the size and weight of a Maine Coon.

2.2 Mechanical Design of Rear Limbs

The mechanical design of the cat robot aims to mimic feline morphology as accurately as possible without introducing unnecessary complexity. For our purposes, this means that the hip, knee, and ankle joints are actuated by motors, and a passively compliant MTP joint allows the foot to conform to the ground throughout stance. Analyses of feline locomotion generally focus on the hip, knee, and ankle, and excludes the MTP joint in the foot [10,31]. Using these active and passive degrees of freedom allows us to capture the main components of locomotion.

The knee and ankle of the robot are simplified to be hinge joints, so each has one motor controlling flexion and extension. The hip in the animal is a ball-and-socket joint, though it has been shown that motion in the sagittal plane alone is sufficient to produce locomotive behavior [25]. However, it was found that abduction/adduction motion in the hip plays a significant role in the stability of walking [25,28]. Therefore, we have included motors to control motion of the hip joints in both the sagittal and frontal planes of motion. Future works may require a redesign of the ankle to include additional degrees of freedom.

Final Design. Our final design is scaled up by a factor of 1.75 from the size of the biological cat used in our torque analysis. This places our design within the acceptable limits of the torque capabilities of the motor as discussed in the Sect. 2.1. We decided to implement a belt-driven system, with a motor at the hip actuating the knee, and motor at the knee actuating the ankle. Thus, there is no concentrated mass load at the end of the tibia, reducing the inertia of the leg with respect to the hip joint.

Our belt-drive system uses Fingertech timing belts (Fingertech Robotics Ltd., Saskatoon, CA), with custom 3D-printed gears adapted from the Fingertech 16T gears. The gear ratio from driving motor at the hip to actuated joint at the knee is 1:1, as is the gear ratio from the driving motor at the knee to the actuated joint at the ankle. The purpose of having the ankle and knee belt-driven is to allow for the motors to be placed higher up on the limb, reducing the inertia of the robot about the hip. The Koala BEAR motors do not have a driveshaft. Rather, they have an actuated faceplate to which objects can be fastened. Our driving gears were adapted to bolt directly to the faceplate, with mounting holes matching that on the faceplate of the motor. These gears were 3D printed without supports.

The current version of the cat robot, depicted in Fig. 1, consists of only the rear limbs, so the pelvis need not be fully actuated or anatomically accurate. As we have no front limbs to support the robot, the pelvis is currently mounted to a platform with two vertical rods, with ball bearings ensuring smooth vertical motion. For ease of design, manufacturing, and to provide a place to mount electronics, the base of the pelvis consists of a flat plate with two large holes cut out for placement of linear ball bearings, and eight smaller holes above the point where the abduction/adduction motor is mounted. The motor is attached to the bottom of the pelvis, enclosed in a 3D-printed structure with tapped M3 holes so that the full weight of the motor is not being supported by the four M3 mounting holes on its top face.

An enclosure for the flexion/extension motor mounts directly to the faceplate of the abduction/adduction motor. Mounted to the flexion/extension motor is a connector piece, which creates an offset between the head of the femur and the outside of the pelvis in order to allow the femur to rotate 360° without contacting the pelvis when the flexion/extension motor is vertical.

Femur. The final femur design is shown in Fig. 3. The eight holes on the face of the head of the femur allow it to mount directly to the connector piece, and thus it is directly driven by the flexion/extension motor. A belt channel runs through the center of the femur, with significant cutouts along the shaft to allow for easy access to and maintenance of the timing belt and gears. The cutouts along the shaft are also far enough apart to accommodate the head of the tibia, which mounts at the circular hole at the distal end of the femur. The platform extending out from the head of the femur houses the motor, which is bolted on from below and is used to belt-drive the knee.

Tibia. The head of the tibia is longer than that of the femur so that there is room for both the driven gear (at the point where the D-slot is located) and the driving gear within the head of the tibia. Because providing enough vertical clearance to prevent collision of the bottom of the femur and the top of the knee-mounted motor would require that the motor be placed too low on the tibia, the motor is mounted at a 5 mm offset from the face of the head of the tibia to

allow full range of motion of the tibia about the knee. Aside from the changes mentioned above, the tibia design is largely the same as the femur design.

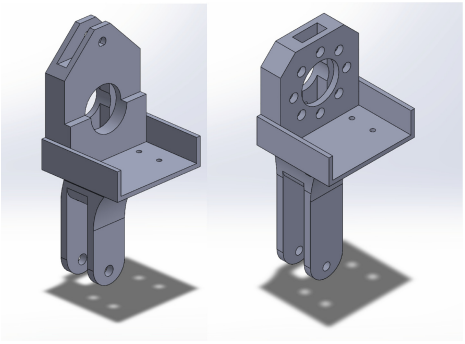

Fig. 3. Left: Isometric view of robot tibia. Right: Isometric view of robot femur.

2.3 Mechanical Design of the Foot

While many quadrupedal robots exist, few use compliant mechanisms for their feet. Most quadrupedal robots use peg or rounded ball feet for simplicity [17]. However, these designs do not move like the feet of a cat. A compliant foot design may enable the cat robot to better mimic cat gait by allowing the foot to conform to the ground throughout stance without the additional complexity of a fully actuated foot. It has also been shown that the use of passive compliance in the feet of robots increases the stability of the robot [3,4,27]. The compliant foot must be compatible with the femur and tibia described above. It must be able to handle stresses during locomotion and have a range of motion comparable to that of a biological cat.

Before generating concepts for the compliant foot design, we conducted research on cat anatomy and preexisting robotic feet [5,14]. The hind feet of a cat have three main sections: the tarsals, metatarsals and the phalanges [6]. The basic shape of the compliant foot was designed to closely approximate the shape of a biological cat foot, with a focus on retaining the joint between the tarsals and phalanges. For ease of manufacturability and stability, the design does not include individual movable toes.

We chose a design which used silicone rubber as a passive spring housed between the digits and tarsals. The toe and tarsal sections of the hind foot were fabricated as separate parts and joined through casting silicone in an appropriate shape. The shape of the toe and tarsal components was modified in consideration for the appropriate range of motion for the hind foot. The foot is expected to have a joint range of 0 to 90°.

Mathematical Models. To analyze the flexure and stress of the joint, we modeled the compliant foot as a small-length flexural pivot [20]. Using a beam length of L and a flexural segment of length l, the stiffness, movement, and stress can be modeled using the following equations:

$$c = \frac{h}{2} \tag{8}$$

$$\theta_0 = \frac{M_0 l}{EI} \tag{9}$$

$$K = \frac{EI}{l} \tag{10}$$

$$\sigma_{max} = \frac{M_0 c}{I} \tag{11}$$

where c refers to half of the beam height, I refers to the area moment of inertia, M_0 refers to the moment applied at the end of the beam, and E is the Young's modulus. The moment approximation was used due to available estimated motor torques. Based on the joint torque calculated for the ankle motor, a moment value of 0.744 N $\cdot$ m was used. The silicone beam length, width, and height were chosen based on its fit in the tarsal and toe components. The beam length is approximated using the length of the tarsal component, as the moment is applied from the end of the tarsal. Table 2 lists these values used in this model. Using this model, we calculated a stress of 2.3 MPa at the joint. These equations are rough approximations, especially for the degree of bending observed during prototyping. However, they were deemed close enough for initial design (Fig. 4).

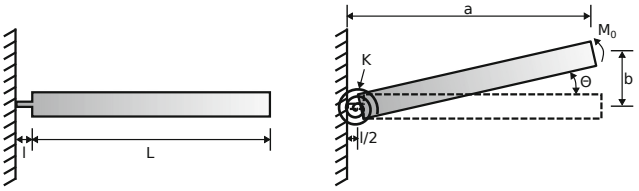

Fig. 4. Pseudo Rigid Body Model of Small Length Flexural Pivot [20].

Table 2. Values used for the model of the Metatarsophalangeal Joint.

Parameter	Value
Moment, M_0	0.744 Nm
Beam Length, L	0.107 m
Silicone Length, l	0.015 m
Silicone Width, w	0.016 m
Silicone Height, h	0.0115 m
Area Moment of Inertia, I	2.03E−9 kg $\cdot$ m^4
Neutral Axis Location, c	0.0125 m

The dimensions of the compliant foot are based on data obtained from a biological cat. The robot is scaled to 1.75 times the size of this cat, so the tarsal and toe components were restricted to 0.108 m and 0.048 m long, respectively.

We modeled the silicone joint concept in SolidWorks. The phalanges were grouped together as a single toe component. The tarsals and metatarsals were grouped together as one tarsal component. The end of the toe component which faces the tarsal has a curve to guide the movement range of the tarsal. In order to decrease stress on the overhang, we added a flare to the end of the tarsal which faces the toe. This spreads out the area that the tarsal is in contact with the toe component when the joint is in a 90° position.

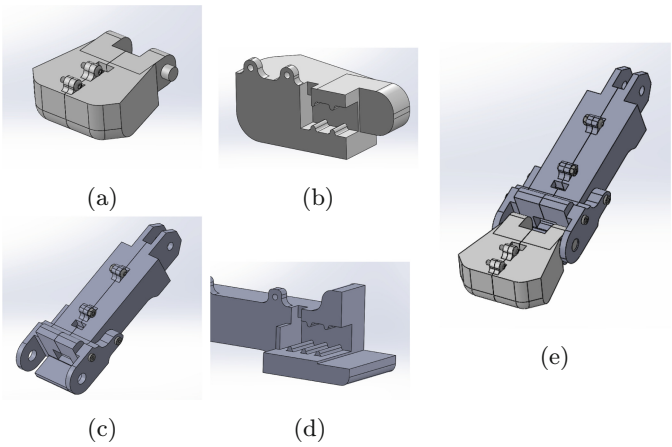

Fig. 5. Tarsal model with compliant MTP joint. (a) Toe Component. (b) Cut view of toe. (c) Tarsal component. (d) Cut view of tarsal. (e) Fully assembled tarsal model with compliant MTP joint.

Both the toe and tarsal components include a hollow chamber for the silicone rubber. We added teeth to both chambers to grip the silicone and prevent it from sliding out after casting. There are 4 teeth in the chamber in the toe, with two on the top and two on the bottom. There are 5 teeth in the tarsal chamber, with two on the top and three on the bottom. These teeth are rounded to prevent potential tear damage. These features as well as the assembled model of the tarsal and toes is shown in Fig. 5

Materials. We 3D printed the main components of the compliant foot for ease of manufacture. Dragon Skin brand (Smooth-On, Macungie, PA) silicone rubber was chosen for use at the joint due to its flexibility and durability. This brand of silicone is located on the middle to lower range of the hardness scale, which allows it the flexibility to bend without cracking. In addition, it has the strength to withstand the expected loads on the joint. We bought and tested 3

variants of Dragon Skin silicone rubber—Dragon Skin 10 Medium, Dragon Skin 20, and Dragon Skin 30—to compare their characteristics. These variants were chosen due to their tensile strength being higher than the stress we calculated of 2.3 MPa. A simplified list of their properties is shown in Table 3. In addition, the torsional stiffness was estimated for all three variants using the first iteration of the foot. These estimated values were calculated by measuring the bend angle of the foot under the weight of the tarsal.

Table 3. Silicone Rubber Properties [32].

Variant	Hardness	Cure Time (h)	Tensile Strength (MPa)	100% Modulus (E, MPa)	Estimated Torsional Stiffness (K, N*m/rad)
Dragon Skin 10	10 A	5	3.275	0.152	0.0128
Dragon Skin 20	20 A	4	3.792	0.338	0.0110
Dragon Skin 30	30 A	16	3.447	0.593	0.104

In the end, Dragon Skin 30 was chosen for the joint, as Dragon Skin 10 and 20 both had very similar torsional stiffness, and occasionally remained in a bent configuration rather than returning to a flat configuration when the foot was moved around. Additionally, the weight of the tarsal component alone was able to bend the 10 and 20 feet a significant amount ($>70°$), which meant that they are too compliant and would not hold up well under the weight of the full robot. While the material of the foot should be able to handle the stresses from the robot weight itself, the bending mechanism would not behave as desired. In this scenario, the foot may immediately go from a 0 to 90° configuration without much resistance. In comparison, Dragon Skin 30 was stiff enough to return to a flat configuration after bending in preliminary tests, and the weight of the tarsal component only bent the foot below 45°. Additionally, the amount of silicone in the foot can be adjusted to the stiffness needs of the robot in future designs.

3 Results

Before beginning experiments with the cat robot, we implemented a simulated model of our design in the physics simulator Mujoco [35]. This model allowed us to validate the joint controller which will be used to control the robot, and to get an idea of the results we could expect from our Koala BEAR motors.

One of the primary motivations behind using quasi-direct drive actuators for our robot was their ease of torque control [30], which allows us to dynamically adjust the stiffness and damping of any joint on the robot in order to test theories about dynamic scaling in animal joints. We can do this by directly controlling the torque at each joint to mimic a rotational system with stiffness and damping

$$\tau = -k \cdot (\theta - \theta_0) - c \cdot \dot{\theta} \tag{12}$$

where θ is the motor position, θ_0 is the motor resting position, $\dot{\theta}$ is the motor velocity, k is the rotational stiffness coefficient, c is the rotational damping coefficient, and τ is the motor torque. As the focus of these simulations was on the motor controller, a more traditional, rigid foot was used rather than the foot with compliant toes. Further testing will be done to evaluate various designs of the feet as they relate to the normal gait cycle.

We subjected the simulated leg to multiple drop tests where the leg fell from a height of 0.55 m and collided with the ground. For each test we varied the stiffness and damping coefficients for all of the joints. Results can be seen in Fig. 6. The simulations use a forward Euler method, with a time step matching a reasonable control frequency for the motors [24,30]. As expected, setting the stiffness to large values results in underdamped oscillations and setting the damping to large values results in an overdamped behavior.

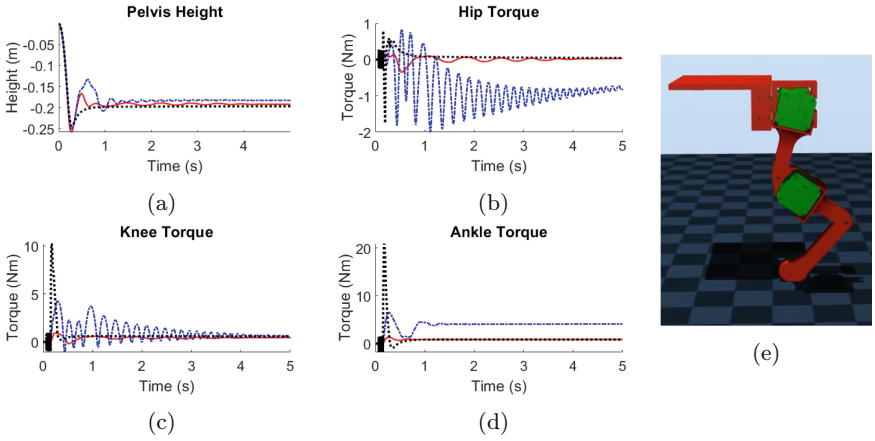

Fig. 6. Simulated leg with joints exhibiting controlled stiffness and damping. **A.** Pelvis height during drop tests. **B–D.** Hip, Knee, and Ankle motor torques during drop tests. **E.** Simulated robot leg in Mujoco [35]. In the simulation, each motor rotates, and the pelvis translates vertically. Three drop tests with varying stiffness and damping: Red solid line: $k = 1$, $c = 0.001$; Blue dashed line: $k = 5$, $c = 0.001$; Black dotted line: $k = 1$, $c = 1$.

4 Conclusions and Further Work

This paper has outlined the design of a robotic hindlimb similar to that of a domestic cat. The hindlimb was designed at 1.75 scale of a normal cat. This was chosen to allow sufficient space to fit the motors while ensuring the increased joint torques do not exceed their capabilities. The initial simulations of the robot performing a drop test show that the motor control code is capable of adapting

its stiffness and damping properties. However, the overdamped system results in peak ankle torques of around 20 Nm (Fig. 6d, black dotted line), while the motors peak at 10.4 Nm. Further testing will be done to compare the limits of the stiffness and damping properties and compare the simulated results to the physical robot. A preliminary design of a foot with compliant toes has also been outlined, with the compliant mechanism coming from silicone cast into a 3d printed limb. This will allow the foot to conform to the ground, remaining in contact with the ground throughout the stance phase.

Our future work with the cat robot shall progress in several stages. Upon construction of a complete rear of the cat robot, we will begin to validate an existing neural model of mammalian hindlimb locomotion [8], using data from our partners at Georgia Tech to ensure that the robotic cat's motion is true to that of the cat it is based upon. While validation of the rear of the cat is in progress, research and design efforts will begin for the front of the cat robot. The primary design is the floating scapula to which the rest of the forelimb is anchored. Prior work with cat robots has ignored the floating scapula in favor of a fixed shoulder joint (with one exception [12]), and thus this is a novel area of development. As the mechanics of the robot must reasonably emulate the biomechanics of the cat in order for the robot to be useful in animal-like experimentation, a workable facsimile of the floating scapula is crucial to our goals.

In addition to this continuation of prior work, we have several goals specific to this robot. We aim to explore the impact of various elastic and damping properties on the motion of our robot, with two intended outcomes. First, we aim to determine how different combinations of anatomy and nervous system construction perform. For example, what exactly goes wrong if a robot with the dynamic properties of a cat tries to move like a praying mantis? Secondly, we intend to evaluate the usefulness of passive elements in helping a robot achieve biomimicry in its locomotion. This will aid future roboticists in design decisions, as it will provide insight into interactions between the neural controller and the mechanical system it controls.

In the long term, we aim for the cat robot to be able to walk independently of an external support structure. This will allow us to better replicate prior work in feline biomechanics, as it will increase the range of possible movements achievable by our cat robot. For one such planned experiment, a split-belt treadmill is being built in the lab to capture and verify the ground reaction forces of the robots being tested. The treadmill will record data for speeds up to 1 m per second, and will be able to collect limb data for both left and right limbs simultaneously and independently. Each side of the treadmill will be able to change speed and direction independently of each other [9], which helps with testing inter-limb coordination of the cat robot [11], thus allowing us to simultaneously validate the accuracy of our mechanical design and our controller.

Acknowledgments. We would like to thank the Biomechanics and Motor Control Lab at Georgia Tech for providing access to the data from their work.

References

1. Ache, J., Matheson, T.: Passive joint forces are tuned to limb use in insects and drive movements without motor activity. Curr. Biol. **23**(15), 1418–1426 (2013)
2. Aronhalt, E.R.: Development of a robotic rat hindlimb model and neural controller (2023)
3. Beer, R.D., Quinn, R.D., Chiel, H.J., Ritzmann, R.E.: Biologically inspired approaches to robotics: What can we learn from insects? Commun. ACM **40**(3), 30–38 (1997)
4. Catalano, M.G., et al.: Adaptive feet for quadrupedal walkers. IEEE Trans. Robot. **38**(1), 302–316 (2021)
5. Chatterjee, A., Mo, A., Kiss, B., Gonen, E.C., Badri-Sprowitz, A.: Multi-segmented adaptive feet for versatile legged locomotion in natural terrain. In: Proceedings - IEEE International Conference on Robotics and Automation 2023-May, pp. 1162–1169 (2022)
6. Coulson, A., Lewis, N.: An Atlas of Interpretative Radiographic Anatomy of the Dog and Cat. Wiley (2002)
7. Day, L.M., Jayne, B.C.: Interspecific scaling of the morphology and posture of the limbs during the locomotion of cats (Felidae). J. Exp. Biol. **210**(4), 642–654 (2007)
8. Deng, K., Szczecinski, N.S., Arnold, D., Andrada, E., Fischer, M.S., Quinn, R.D., Hunt, A.J.: Neuromechanical model of rat hindlimb walking with two-layer cpgs. Biomimetics **4**, 21 (2019)
9. Dimiskovski, M., Scheinfield, R., Higgin, D., Krupka, A., Lemay, M.A.: Characterization and validation of a split belt treadmill for measuring hindlimb ground-reaction forces in able-bodied and spinalized felines. J. Neurosci. Methods **278**, 65–75 (2017)
10. Ekeberg, Ö., Pearson, K.: Computer simulation of stepping in the hind legs of the cat: an examination of mechanisms regulating the stance-to-swing transition. J. Neurophysiol. **94**, 4256–4268 (2005)
11. Frigon, A., Hurteau, M.F., Thibaudier, Y., Leblond, H., Telonio, A., Angelo, G.D.: Split-belt walking alters the relationship between locomotor phases and cycle duration across speeds in intact and chronic spinalized adult cats (2013)
12. Fukuhara, A., Gunji, M., Masuda, Y., Tadakuma, K., Ishiguro, A.: Flexible shoulder in quadruped animals and robots guiding science of soft robotics. J. Robot. Mechatron. **34**, 304–309 (2022)
13. Goldsmith, C.A., Szczecinski, N.S., Quinn, R.D.: Neurodynamic modeling of the fruit fly drosophila melanogaster. Bioinspiration Biomimetics **15**, 065003 (2020)
14. Goldsmith, C.A., Zyhowski, W.P., Büschges, A., Zill, S.N., Dinges, G.F., Szczecinski, N.S.: Effects of tarsal morphology on load feedback during stepping of a robotic stick insect (carausius morosus) limb. In: Lecture Notes in Computer Science (Including Subseries Lecture Notes in Artificial Intelligence and Lecture Notes in Bioinformatics), 14157 LNAI, pp. 442–457 (2023)
15. Griffin, C., Choong, W.Y., Teh, W., Buxton, A.J., Bolton, P.S.: Head and cervical spine posture in behaving rats: implications for modeling human conditions involving the head and cervical spine. Anat. Rec. **298**(2), 455–462 (2015)
16. Günther, M., Rockenfeller, R., Weihmann, T., Haeufle, D.F., Götz, T., Schmitt, S.: Rules of nature's formula run: Muscle mechanics during late stance is the key to explaining maximum running speed. J. Theor. Biol. **523**, 110714 (2021)
17. Hauser, S., Eckert, P., Tuleu, A., Ijspeert, A.: Friction and damping of a compliant foot based on granular jamming for legged robots. In: Proceedings of the IEEE RAS

and EMBS International Conference on Biomedical Robotics and Biomechatronics, 2016-July, pp. 1160–1165 (2016)
18. Hooper, S.L.: Body size and the neural control of movement. CURBIO **22**, R318–R322 (2012)
19. Hooper, S.L., Guschlbauer, C., Blümel, M., Rosenbaum, P., Gruhn, M., Akay, T., Büschges, A.: Neural control of unloaded leg posture and of leg swing in stick insect, cockroach, and mouse differs from that in larger animals. J. Neurosci. **29**(13), 4109–4119 (2009)
20. Howell, L., Magleby, S., Olsen, B.: Handbook of Compliant Mechanisms. John Wiley & Sons (2013)
21. Hunt, A., Szczecinski, N., Quinn, R.: Development and training of a neural controller for hind leg walking in a dog robot. Front. Neurorobot. **11**, 18 (2017)
22. Ilton, M., et al.: The principles of cascading power limits in small, fast biological and engineered systems. Science **360**, eaao1082 (2018)
23. More, H.L., Maxwell, D.J.: Scaling of sensorimotor delays in terrestrial mammals. Proc. R. Soc. B. **285**, 20180613 (2018)
24. Liu, Y., Shen, J., Zhang, J., Zhang, X., Zhu, T., Hong, D.: Design and control of a miniature bipedal robot with proprioceptive actuation for dynamic behaviors. In: 2022 International Conference on Robotics and Automation (ICRA), pp. 8547–8553
25. Lyakhovetskii, V.A., Gorskii, O.V., Gerasimenko, Y.P., Musienko, P.E.: Mathematical model of the hindlimbs control during cat locomotion with balance. Rossiiskii Fiziologicheskii Zhurnal Imeni IM Sechenova **101**(2), 200–213 (2015)
26. Mangan, M., et al.: A virtuous cycle between invertebrate and robotics research: perspective on a decade of living machines research (2023)
27. Melo, K., Horvat, T., Ijspeert, A.J.: Minimalist design of a 3-axis passive compliant foot for sprawling posture robots. In: 2019 2nd IEEE International Conference on Soft Robotics (RoboSoft), pp. 788–794. IEEE
28. Misiaszek, J.E.: Control of frontal plane motion of the hindlimbs in the unrestrained walking cat. J. Neurophysiol. **96**(4), 1816–1828 (2006)
29. Prilutsky, B.I., Sirota, M.G., Gregor, R.J., Beloozerova, I.N.: Innovative methodology quantification of motor cortex activity and full-body biomechanics during unconstrained locomotion (2005)
30. Seok, S., Wang, A., Otten, D., Kim, S.: Actuator design for high force proprioceptive control in fast legged locomotion. In: IEEE International Conference on Intelligent Robots and Systems, pp. 1970–1975 (2012)
31. Shen, L., Poppele, R.E.: Kinematic analysis of cat hindlimb stepping. J. Neurophysiol. **74**, (1995)
32. Smooth-On: Dragon skin ™series. https://www.smooth-on.com/product-line/dragon-skin/
33. Sutton, G.P., Szczecinski, N.S., Quinn, R.D., Chiel, H.J.: Phase shift between joint rotation and actuation reflects dominant forces and predicts muscle activation patterns (2023)
34. Szczecinski, N.S., et al.: Introducing mantisbot: Hexapod robot controlled by a high-fidelity, real-time neural simulation. In: IEEE International Conference on Intelligent Robots and Systems, 2015-December, pp. 3875–3881 (2015)
35. Todorov, E., Erez, T., Tassa, Y.: Mujoco: a physics engine for model-based control. In: IEEE International Conference on Intelligent Robots and Systems, pp. 5026–5033 (2012)